



ARCHIVES  
of  
FOUNDRY ENGINEERING

ISSN (2299-2944)  
Volume 2020  
Issue 1/2020

84 – 94

10.24425/afe.2020.131288

15/1



Published quarterly as the organ of the Foundry Commission of the Polish Academy of Sciences

# Optimization of Al-Cu Cast Alloy Composition for Hydraulic Valves

Rong Li <sup>a,\*</sup>, Lunjun Chen <sup>b</sup>, Qi Zeng <sup>c</sup>, Ming Su <sup>a</sup>, Zhiping Xie <sup>a</sup>

<sup>a</sup> School of Mechanical & Electrical Engineering, Guizhou Normal University, Guiyang, Guizhou, 550025, China

<sup>b</sup> Guizhou University, Guiyang, Guizhou, 550025, China

<sup>c</sup> Guiyang Huaheng Mechanical Manufacture CO.LTD, Guiyang, Guizhou, 550014, China

\* Corresponding author: E-mail address: lirong9242001@163.com

Received 03.09.2019; accepted in revised form 01.12.2019

## Abstract

In order to identify the influence of different Mn, Cd, V and Zr content on the properties of Al-Cu casting alloys in hydraulic valves, orthogonal test methods were used to prepare alloy test bars with different elements and contents. Tensile tests were performed on the test bars so obtained. The microstructure of alloys with different compositions is studied. The results show that adding approximately 0.4% of Mn can not only form a strengthening phase but also reduce the excessive segregation of the matrix along the grain boundary. A Cd content of 0.2% can promote the formation of micro Cd spheres in the softer aluminum matrix. Hard spots increase the wear resistance of the material; however, an excess of Cd will cause element segregation and deteriorate the mechanical properties of the valve body. Zr and V refine the grains in the alloy; however, an excess of these elements will lead to a large area of segregation. If proper heat treatment is lacking, the mechanical properties of the valve body deteriorate.

**Keywords:** Al-Cu cast alloy, Element optimization, Strengthening mechanism, Hydraulic multi-way valve

## 1. Introduction

A multi-way valve is a key component in engineering machinery. The flow in the valve is complex and the fabrication is not easy. Most multi-way valve bodies are made using cast iron [1, 2]. However, high casting temperature causes the core sand to adhere to the body, which would result in the failure of the hydraulic system. An aluminum alloy with well-balanced strength, plasticity, and wear resistance would be a suitable material for hydraulic multi-way valve body.

The 2XXX series Al-Cu alloys have superior mechanical properties and are widely used in engineering applications [3, 4]. Micro alloying with different elements is an important method for reinforcing material properties. Many scholars have studied the effect of Mn, Cd, Zr, V, and other elements in reinforced aluminum alloys. Guoxin Zhang et al. concluded that adding

moderate amounts of Zr to aluminum alloy would refine the microstructure and improve the hardness, tensile strength, and elongation [5]. Y.Y. Li et al showed experimentally that adding Zr and V to aluminum-copper alloy could significantly improve the tensile strength and elongation of the material [6]. However, the strengthening effect of Cd on aluminum alloy has been understood by scholars for a long time, and the strengthening mechanism of the alloy was not fully understood. Moreover, combinations of other elements that enhanced the alloy performance was not found in literature.

This study is based on the 2XXX series of aluminum-copper alloys, and the content of manganese (Mn), cadmium (Cd), vanadium (V), and zirconium (Zr) were adjusted to obtain the optimum proportion of elements for the required mechanical property profile. Subsequently, the strengthening mechanism of the element also was discussed. The optimized alloy would satisfy the requirements of a hydraulic multi-way valve body.

## 2. Experimental Procedure

### 2.1 Experimental methods

In order to identify the optimum composition, the tensile strength and elongation of materials with different proportions of the four elements were tested by the orthogonal method. The different elements are added in a certain order to prepare the material using the process detailed ahead: Al ingots (double zero) and 4.5% Cu (99.9%, Yunnan Al Co. LTD) by weight were melted in a graphite crucible and the other elements were added to the crucible in different proportions. Subsequently, the Cd

(99.99%, Yunnan Al Co. LTD) was added in the metal form, Zr (4.65%, Chongqin Shunbo), and V (10%, Chongqin Shunbo) were added in the form of intermediate alloys, and Mn was added by agent (75%, Yunnan Al Co. LTD). Cd, Zr, and V were melted with the Al ingots and the Mn was added during the liquid metal refining. The melting temperature is controlled at 650-720 °C after all the alloy elements have undergone smelting, refining, slagging, and resting in the crucible. Thereafter, the refined melt (650 to 700 °C) was cast into a metal test bar mold which has been preheated to 280-320 °C. Hence, an alloy test bar that satisfies the Chinese standard GB/T228-2002 is obtained after opening the mold. The test bar and casting are shown in Figure 1.

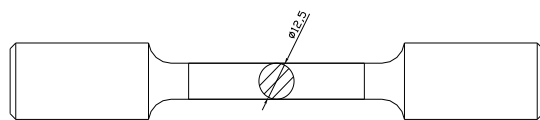


Fig.1. Test bar and its casting

### 2.2 Testing methods

An electronic universal material testing machine (CBW-10T-Chongqing) is used for testing the bar after heat treatment in the T5 state (solution treatment and incomplete artificial aging). An electronic extensometer (Beijing Iron and Steel Research Institute) is used to measure the elongation during tensile testing. An electronic metallurgical microscope (4XC-TV type) was used to observe the metallographic structure of the specimens. Fracture morphology of the test bars after tensile fracture was observed by scanning electron microscopy (KYKY-2800B). The thinned test piece was analyzed by transmission electron microscopy (TEM, Bruker JEM-2100F) to check the structure of the different alloy components and their effects on material properties. Electron probe microscopy is used to test the distribution of elements (EPMA-1720).

## 3. Experimental results

### 3.1 Analysis of Mechanical Behavior

The effects of the different components on the mechanical strength of the material were obtained by orthogonal design experiments. Table 1 shows the tensile strength and elongation of the orthogonal experimental specimens.

Table 1.  
Results of orthogonal experiments with different composition

Specimen	Elements	Mn (wt.%)	V (wt.%)	Zr (wt.%)	Cd (wt.%)	Tensile strength (MPa)	Elongation (%)
No. 1		0.25	0.016	0.1	0.1	322.875	3.371
No. 2		0.25	0.1	0.19	0.2	344.849	2.902
No. 3		0.25	0.15	0.25	0.4	307.552	4.079
No. 4		0.3	0.016	0.19	0.4	271.642	2.237
No. 5		0.3	0.1	0.25	0.1	282.141	3.608
No. 6		0.3	0.15	0.1	0.2	393.128	1.923
No. 7		0.4	0.016	0.25	0.2	415.514	3.445
No. 8		0.4	0.1	0.1	0.4	384.155	3.308
No. 9		0.4	0.15	0.19	0.1	378.254	2.887

Statistical analysis in this case involves range and variance

analysis. Range analysis is simple and intuitive, and can elucidate

the effect of a single element. However, it cannot show the estimated error value. Variance analysis can reflect the fluctuations caused by the different horizontal factors between the different influencing factors and fluctuations caused by test errors within the same group. So, Table 2 and Table 3 show the average strength and elongation of a single element for the various horizontal factors. Also, the range of the test is shown in Table 2 and Table 3, while the Figure 2 shows the average of strength and elongation with different element content.

Range and average strength of various horizontal factors (MPa)

Fact	Mn	V	Zr	Cd
Average 1	325.09	336.68	366.72	327.76
Average 2	315.64	337.05	331.58	384.50
Average 3	392.64	359.64	335.07	321.12
Range	77.00	22.97	35.14	63.38

Table 3.

Range and average elongation of various horizontal factors (%)

Fact	Mn	V	Zr	Cd
Average 1	3.45	3.03	2.87	3.29
Average 2	2.59	3.27	2.68	2.76
Average 3	3.21	2.96	3.71	3.21
Range	0.86	0.31	1.04	0.53

Table 2.

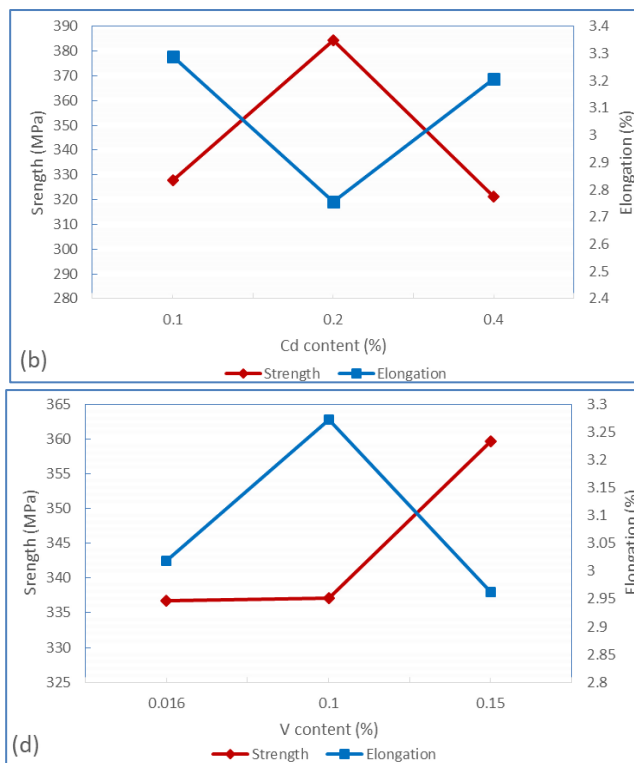
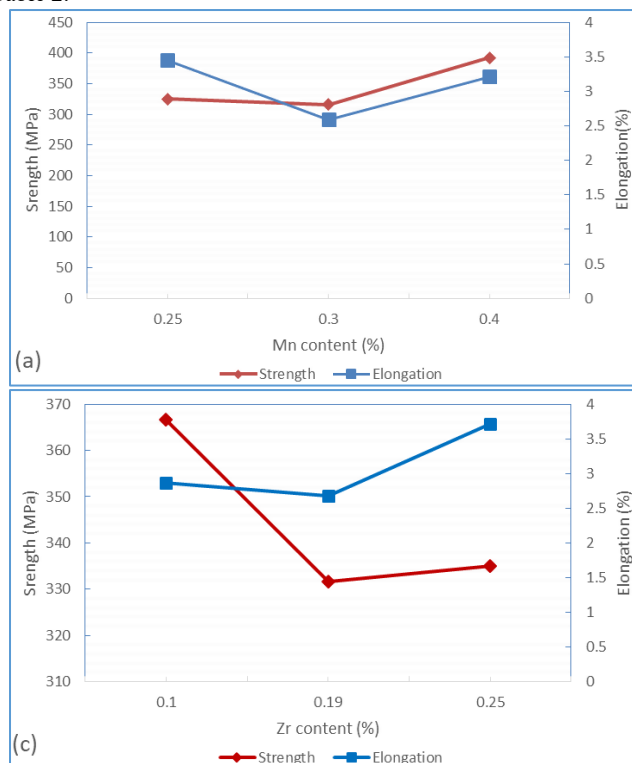


Fig.2. Effect of different element contents on mechanical strength of alloy

One-way ANOVA using SPSS19.0 was used to test the effect of various elements and the results are as shown in Table 4. This

reflects the ANOVA of the tensile strength and elongation of different material specimens.

Table 4.

## One-way ANOVA of variance analysis of orthogonal experiments

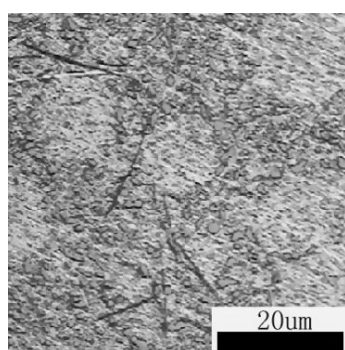
Elements	ANOVA of tensile strength			ANOVA of elongation		
	DEVSQ	df	F	DEVSQ	df	F
Mn	7313.818	2	2.019	1.188	2	1.297
V	1630.691	2	0.450	0.164	2	0.179
Zr	1591.631	2	0.439	1.820	2	1.986
Cd	3951.938	2	1.091	0.493	2	0.538
Deviation	14488.08	8		3.665	8	

From the Table 2 and Table 3, the maximum range of the strength and elongation is exhibited by Mn and Zr. The influence of the elements on the strength of the material in decreasing order were arranged as Mn, Cd, V, and Zr. It can be seen from the results summarized in Table 4. The elongation analysis of variance shows that Zr is most influential for the elongation, followed by Mn, Cd, and V.

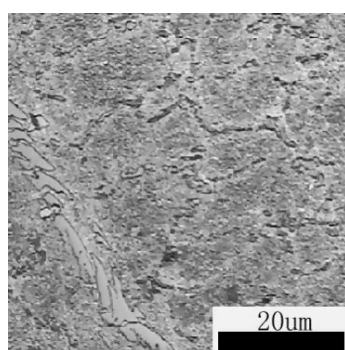
Figure 2 shows the effect of different elements on the mechanical properties of the material. It can be seen from the figure that the element contents have a certain influence on the material. As the Mn content, the strength of the alloy increases continuously (Fig. 2-a). However, the addition of Cd is beneficial only until 0.2%, which corresponds to the optimum strength of the material (Fig. 2-b). The addition of Zr causes the strength to increase slowly when the content is low. Subsequently, the strength drops sharply when the content is 0.25% (Fig. 2-c). The addition of V causes an effect that is opposite to that caused by Zr, which has a lowest strength value at a content of 0.1% (Fig. 2-d). Therefore, from the above results, the elemental composition for obtaining the optimum strength are: Mn-0.4%, Cd-0.2%, Zr-0.19%, and V-0.016%. However, from the result of the elongation analysis, Zr has the greatest influence on the elongation of the material. However, the addition of Zr at 0.1% and 0.19% has no obvious effect on the strength. Considering the balance between material strength and plasticity, the final elemental content of the alloy was determined to be Mn-0.4%, Cd-0.2%, Zr-0.1%, and V-0.016%.

### 3.2 Analysis of Micro Morphology

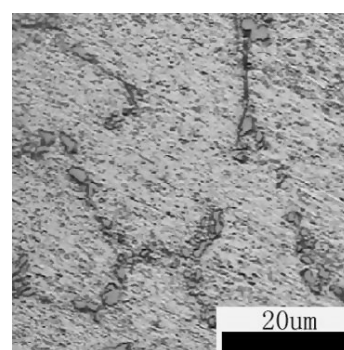
Figure 3 shows the morphology of the material observed by metallographic microscopy after the corrosion of specimens, which is obtained from the orthogonal test. It shows that the metallographic structure is related to the mechanical properties of the alloy. Fig. 3-f shows the metallographic morphology of specimen 6. It can be seen that there is a large piece of contiguous structure, which has a significant influence on the elongation properties of the material. The tensile strength of specimen 4 is the lowest and its metallographic phase was shown in Fig. 3-d. There is a large irregular block structure on the surface. Those irregular block structures cut and split the material matrix, leading to a decrease in the strength of the alloy. It dispersed into a large amount of fine particulate matter and the distribution is relatively uniform as per the metallographic image of specimen 7. Strength properties of this specimen are the best in the tensile regime, but the elongation is slightly insufficient. A narrow black morphology is observed at the metallographic center (Fig. 3-g) and this morphology should be due to segregation. There is a high content of Mn and Cd in specimen 8. A large amount of the strengthening phase was dispersed on the substrate. However, strengthening morphology precipitates along the grain boundary to form a bulk material. This leads to a decrease in the strength of the material.



(a) Specimen 1



(b) Specimen 2



(c) Specimen 3

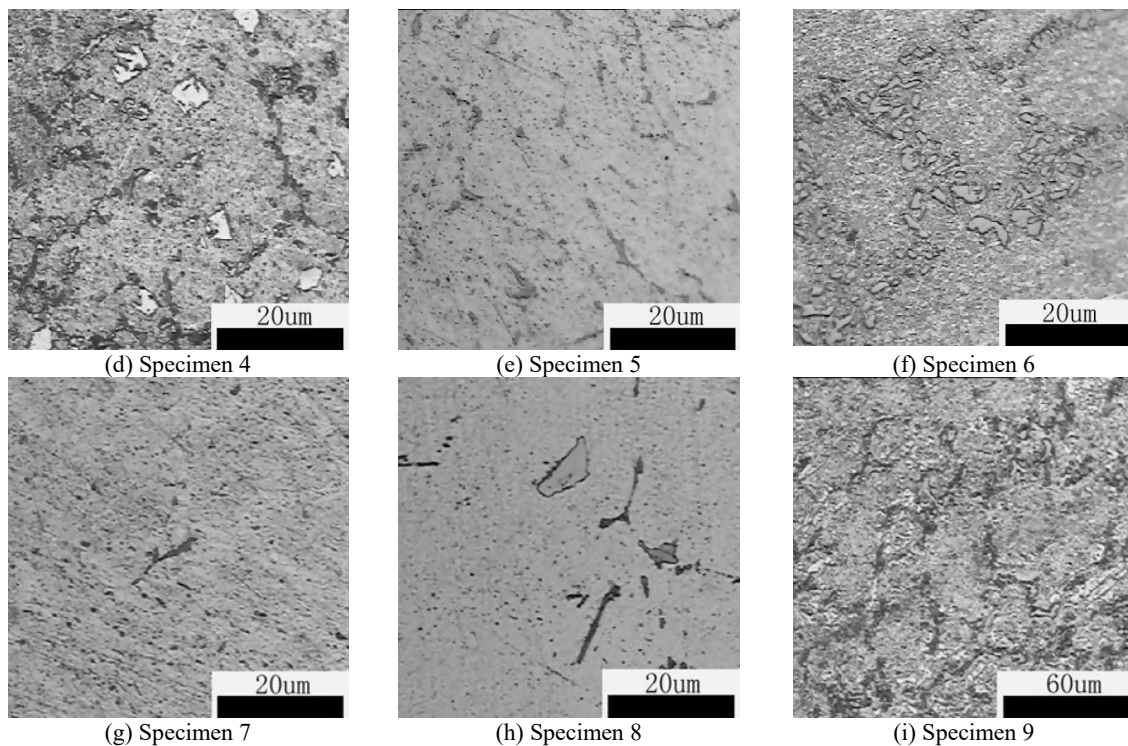


Fig. 3. Metallographic structure of orthogonal experimental specimens

### 3.3 Analysis of Fracture Morphology

SEM of the fracture morphology of Specimen 5 is shown in Figure 4. The macroscopic fracture morphology shows the fracture morphology being non-uniform with many irregular dimples and spines on the Fig. 4-a. Small quantities of flaky morphology are distributed at the bottom of the dimple. It may be due to the tearing of the material during breakage. A portion of Fig. 4-a is enlarged and shown in the Fig. 4-b. There are a large number of bright colored dimples on the surface, which indicates a ductile fracture morphology. Except for the small bright dimples, a small groove is formed in the middle of the dimples. A 4-5 μm micro crack (B zone) can be seen at the bottom edge of the groove. This morphology formation mechanism may be as follows: During tensile testing, micro cracks are formed in the joint region of the second phase and the substrate. As the force

increases, the micro cracks expand along the most vulnerable position (C zone) and the surrounding crystals are also continuously stretched and elongated. Eventually, a transgranular fracture was formed. After a large number of crystals broke, a macroscopic fracture morphology is formed. Therefore, the material displays good plasticity. There is flaky tissue in the macro fracture dimples. This is because the connecting strength between the second phase and the alloy matrix is insufficient, which leads to the second phase spall and decrease in the strength of the material. In addition to the flaky morphology formed by the transgranular fracture, there are many small crystalline granules at the bottom of the flaky structure. It shows an intergranular fracture morphology and exacerbates the tendency of the material to be brittle. Through the above analysis, the alloy as a whole exhibited ductile fracture but also underwent brittle fracture.

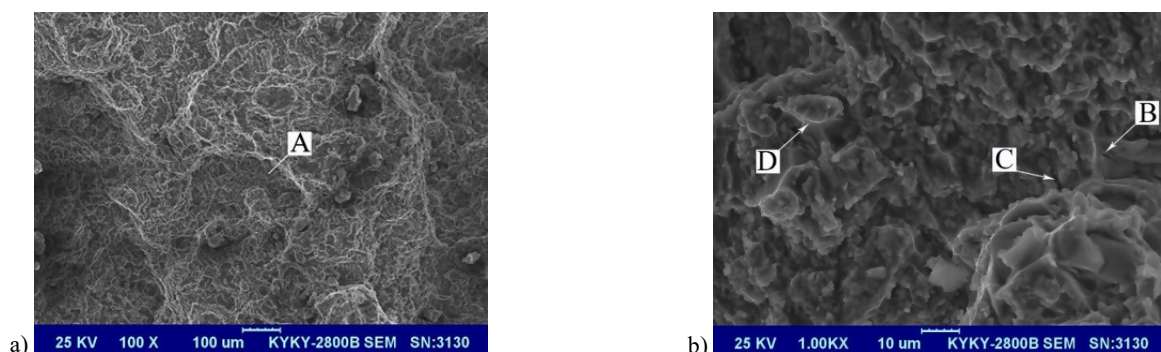


Fig. 4. SEM of fracture morphology of specimen 5

SEM of the fracture morphology of Specimen 7 is shown in Figure 5. It can be seen from the macroscopic morphology of the fracture (Fig. 5.(a)) that the fracture structure of the material is fine and uniform. A large number of small dimples are uniformly distributed, indicating a ductile fracture. After enlarging the A zone, a large number of 2  $\mu\text{m}$  dimples are distributed around the shallow pit, which show a typical transgranular appearance. There is a platform (large rectangular zone in Fig. 5.(b)) in the middle of the shallow pit, which means a large piece of tearing flakes and micro cracks. The bottom of the shallow pit is irregular and extends to the base (small rectangular zone). The material morphology may be formed by this process: the elements surrounding the zone indicated by the rectangles are

uniformly distributed and the strength is better. There may be some segregation of components in the material, which leads to the formation of shallow pits and small platforms. Because the toughness of the platform region is slightly smaller than the others, the interior of the platform starts forming micro-cracks first. Subsequently, the micro cracks expand and finally break. Therefore, there is a large vertical fault zone on the right side of the rectangular platform, and the other positions of the platform are more distributed. The bottom of the shallow pit is irregular and extends to the base (small rectangular zone) as the second phase connected to the substrate cannot withstand the external force and the substrate falls off.

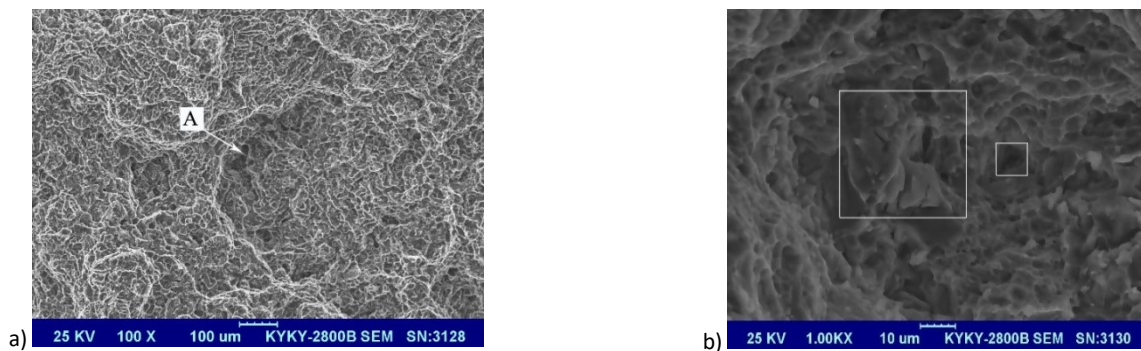


Fig. 5. SEM of fracture morphology of specimen 7

## 4. Results and Discussion

### 4.1 Influence of Mn on alloy strength

The results of the orthogonal experiment indicate that Mn has the greatest influence on the strength of the material. The strengthening mechanism of Al-Cu-Mn alloy is mainly achieved by the formation of solid solution and aging. The mechanism is as follows: firstly, the  $\theta$  ( $\text{Al}_2\text{Cu}$ ) phase is integrated into the matrix

to form a supersaturated solid solution by quenching to achieve solid solution strengthening. Subsequently, a supersaturated solid solution (high concentration) containing Mn and Cu are decomposed and generated at a high temperature. The diffusion migration causes the material to precipitate into a large number of fine and dispersed  $T(\text{Al}_{12}\text{CuMn}_2)$  phase particles, and achieves dispersion strengthening. Finally, the aging treatment causes the Cu solid solution to decompose, and precipitates the GP zone and the  $\theta'$  phase [7]. This process is illustrated in Figure 6.

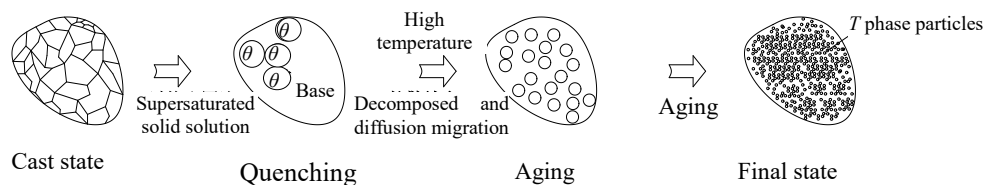
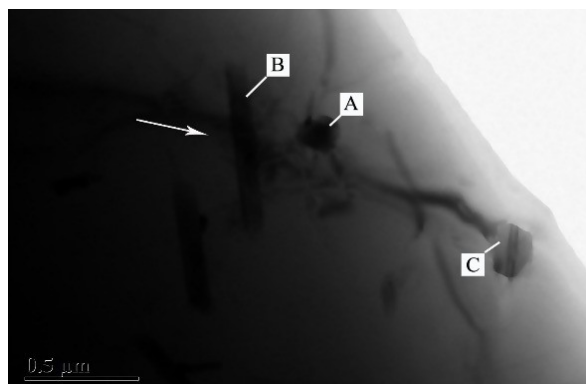


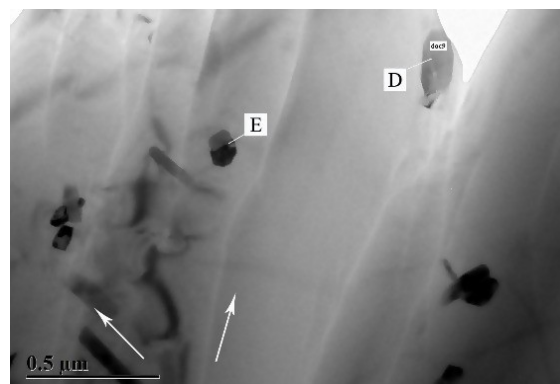
Fig. 6. Process of Mn strengthening

The distribution of Mn inside the material was observed by transmission electron microscopy (TEM). Figure 6 is the TEM images of specimen 7 and specimen 3. From the TEM of the two specimens, it can be seen that there are three different types of

precipitated materials. There are large irregular agglomerations (A position), long rod-shaped substances (B position), and empty tubes (C position and D position) after two phase peeling.



(a) Specimen 7



(b) Specimen 3

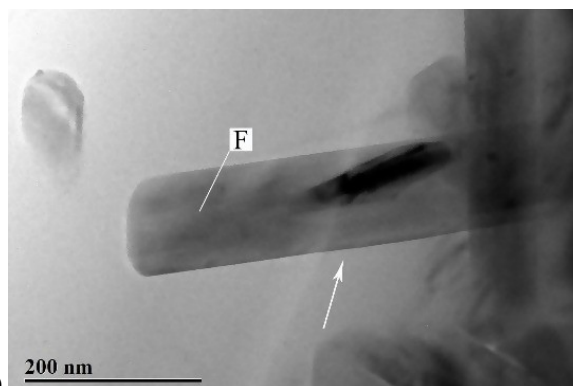
Fig. 7. TEM of specimen

The long rod-shaped region of specimen 7 was enlarged to examine the element composition, and the details are shown in Figure 8 and Table 5. It can be seen that the long rod-shaped region is mainly an Al-Mn-Cu phase, and this Al-Cu-Mn tissue has been embedded in the substrate. The rod-like regions and the substrate are at an inclination to each other as shown by the arrow in Figure 8.

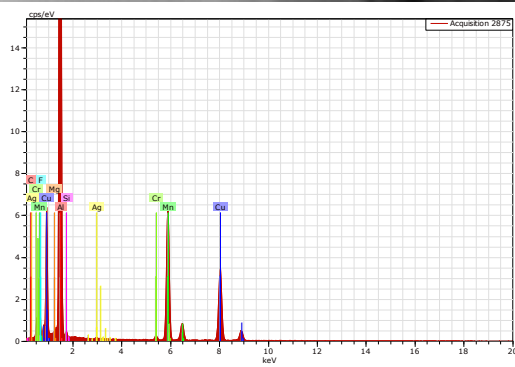
Table 5.

Element content of F point

Element	wt.%	at.%
Al	69.34	82.42
Mn	16.16	9.44
Cu	12.91	6.52



a)



b)

Fig. 8. Enlarged B region and spectrum of specimen 7: (a) TEM of B region, (b) Spectrum of F point

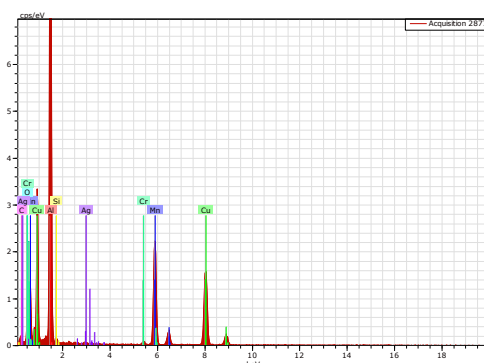


Fig. 9. Magnified view of position D and spectrum of specimen 3

Table 6.

Composition at point D

Element	wt.%	at.%
Al	69.34	82.42
Mn	16.16	9.44
Cu	12.91	6.52

The energy spectrum analysis of the exfoliated tubular region in the D region of specimen 3 revealed that the main component is Al-Mn-Cu, as shown in Figure 9 and Table 6. The magnified view of point E and the energy spectrum analysis are shown in Figure 10 and Table 7. The analysis shows that the main component is Al-Cu. At the same time, the morphology of the area is seen: the black agglomerate phase in the middle, short rod crystal in the upper part, and pleated area of the G point.

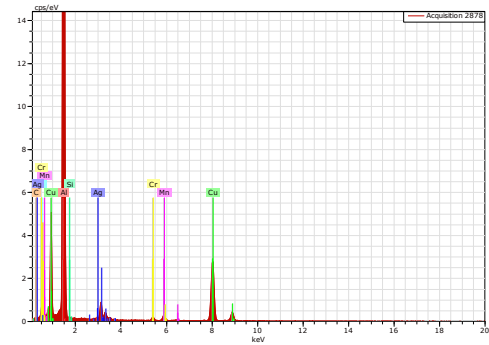
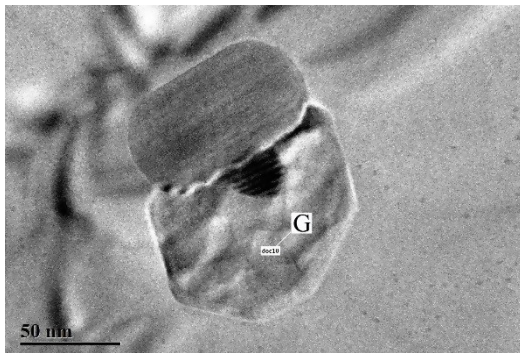


Fig. 10. Magnified view of E Zone and spectrum of specimen 3

Table 7.

Composition of G point

Element	wt.%	at.%
Al	83.32	91.57
Cu	12.68	5.92

The following phenomena can be seen by microscopic analysis of the material:

- 1) The strengthening of Mn is mainly carried out by the Al-Mn-Cu phase, but its state is different. When Mn content is low, the material strengthening is dominated by the  $\theta$  phase and dispersion strengthening due to the  $\theta$  ( $\text{Al}_2\text{Cu}$ ) of the matrix. However, with the increase in Mn content,  $T$  ( $\text{Al}_{12}\text{CuMn}_2$ ) phase strengthening plays a dominant role, forming the GP strengthening that solid solution, dispersion (diffusion) is dominated. Hence, the strengthening phase can be distributed to the maximum. The results also show that the Fig. 3-g of metallographic structure. It causes a significant enhancement in the mechanical properties of the alloy. However, an excessive amount of Mn will cause a large amount of the Al-Mn-Cu phase to precipitate along the crystal. Those elements could alloy with other elements. It will result in a decrease in the mechanical properties of the

material because of the formation of a block tissue and a fractured material matrix. Therefore, there is an optimum value of Mn for the optimum tensile properties of the material. For this material, it is a composition of 0.4% that will provide the optimum performance.

- 2) From the TEM image shown in Fig. 7-b, there is an angle between the long rod-shaped structures and the grain boundary, which is as shown by the arrows in Fig. 6. The long rod-shaped structure is determined to be of the Al-Mn-Cu phase by energy spectrum analysis. This structure can effectively improve the mechanical properties of the material. The micro cracks will be formed initially when the grain boundary and the crystal are being forced. As the force is consistent with the grain boundary and the crystal, the direction of the micro cracks will be the same as the direction of the force. The fracture can be seen in Fig. 4-b. There are long rods, whose direction is perpendicular to the direction of the grain boundary. When the material is tensile, the long rods can act as a beam, and the fiber of the beam is also perpendicular to the force. This structure can bear more force. So, the tensile properties of the material will be improved significantly. The model of the microstructure is shown in Figure 11.

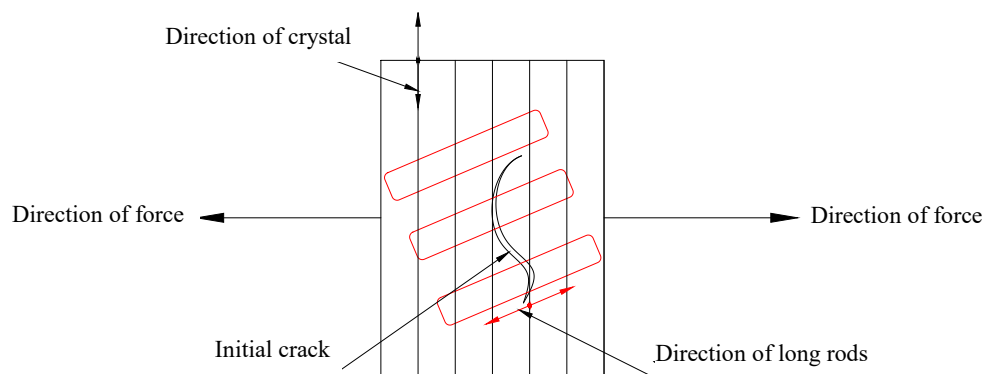


Fig. 11. Fracture model of microstructure

- 3) The significance of the formation of spherical or spheroidal structures on the hydraulic valve body material is explained here. From the TEM display, the addition of Mn will mainly drive the long rod-shaped and spherical or spheroidal tissue forming. For the rod structure, the mechanical strength of

the material can be significantly improved. The spherical structure is more firmly bonded to the substrate due to the larger contact area with the substrate. This performance is suitable for the hydraulic valve because it needs to sustain friction in the long term. During the formation of spheroidal

hard spots, the first contact will be between the point and the surface. These spheroidal hard spots of the alloy material can reduce the abrasion. So, the spherical tissue

could tolerate the friction well. The process of reducing the wear is shown in the Figure 12.

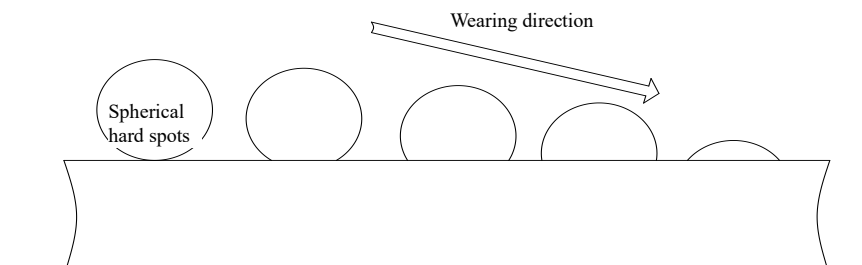


Fig. 12. Model of spheroidal hard spots reduce wear

## 4.2 Influence of Cd on strengthening

Studies have shown that the addition of an appropriate amount of Cd can improve the tensile strength of an Al-Cu alloy [8]. When Cd is added to the alloy, it would accelerate the formation of the GP2 ( $\theta''$ ) and  $\theta'$  phases during the artificial aging process after quenching. It could enhance the strength of the alloy. When the content of Cd is low in the alloy, it will integrate into the  $\alpha$  (Al) phase, while the Cd will be distributed in the dendrite and grain boundaries with the  $T$  phase and the  $\theta$  phase by the formation of spherical particles. It will increase the resistance of the boundary movement, which acts to strengthen the alloy [9, 10]. Figure 13 is the TEM image of specimen 7. It shows a spherical Cd group of approximately 50 nm. After the energy spectrum analysis of the point, it is found that the region is mainly composed of Al-Cd (small amount of Cu, Mn).

Table 8.

Composition at doc16 region

Element	wt. %	at. %
Cd	44.64	17.96
Al	43.54	72.96
Cu	6.82	4.85
Mn	4.09	3.37

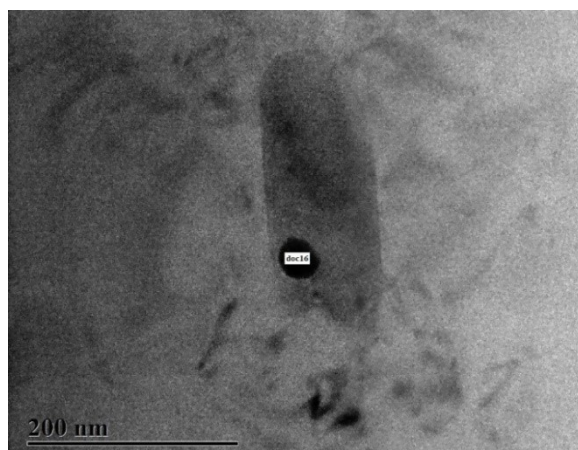


Fig. 13. TEM of spherical Cd

On examining the mechanical properties associated with different Cd compositions, 0.2% Cd obtains the best mechanical properties. If the Cd content is too small, it cannot cause a nailing effect on the grain boundaries to hinder the movement of the grain boundaries. However, the excessive Cd cannot integrate into  $\alpha$  (Al) phase completely and a large amount of Cd will be clustered on the dendrites or grain boundaries. It will result in the formation of a large Cd agglomeration, which will split the alloy matrix, thereby degrading the mechanical properties. It is verified in the metallographic image of Fig. 3-c, Fig. 3-d, and Fig.3-h.

## 4.3 Strengthening by V

Figure 14 shows the electron probe analysis of Specimen 2. The element distribution and composition is observed. Figure 15 shows the electron probe analysis of specimen 1. The difference between both the specimens is mainly in the added V content. It can be seen that there is a large strip of material in the specimen 2, which is close to the metallographic structure of Fig.3-b. However, as shown in Figure 15, specimen 1 does not have a continuous block structure, while the microstructure is fine. The tensile test results also show the effect of the addition of V on the mechanical properties of the material. Excessive V content will cause the material to precipitate in a coarse phase, which leads to the decrease in material strength.

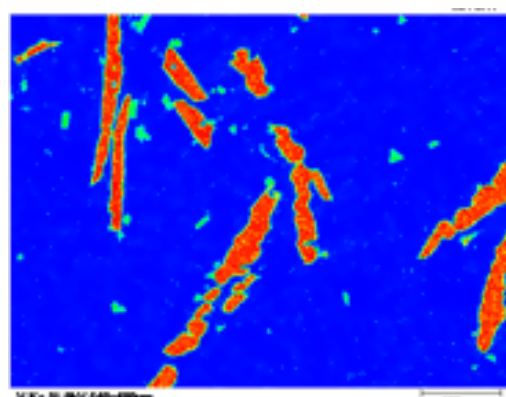


Fig. 14. Electron probe of specimen 2

Table 7.

Composition at point A

No.	Elem	Wt%	Mol%
1	Al	52.7	67.4
2	V	39.36	26.86

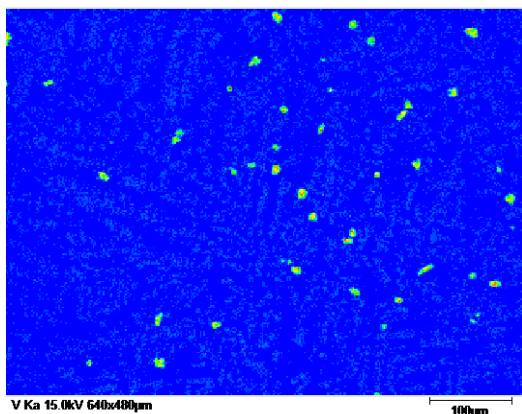


Fig. 15. Electron probe of specimen 1

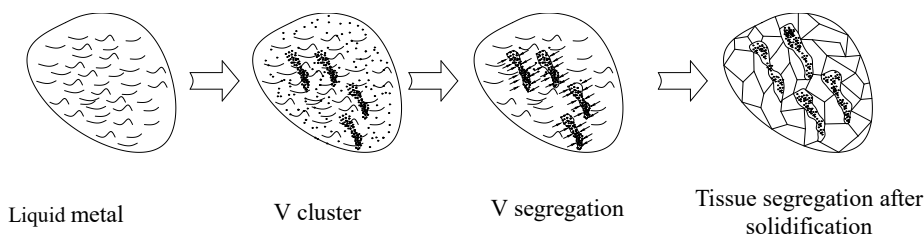


Fig. 16. Process of V segregation

## 5. Conclusions

- 1) Mn can form a long rod-shaped structure by combining with the Al-Cu element and form a certain angle with the fiber. It can resist the expansion of the micro crack and enhance the mechanical properties of the material remarkably.
- 2) The addition of either Mn or Cd results in the formation of a special structure in the matrix. Special hard spots will be formed in the material matrix, which will augment the wear resistance of the material.
- 3) Appropriate quantities of Zr and V help in grain refinement and improve the strength. However, excessive amounts of Zr and V will lead to segregation during solidification and reduce the strength of the alloy.

Most hydraulic valve bodies were manufactured using cast iron or forged steel. After forming, the internal structures made using the hydraulic system process. Medium or large hydraulic valves can be made by integral casting of the assembled pieces, enabling the formation of complex flow paths. Multi-way valves are also fabricated by assembling cast iron parts. However, these assembled valves inevitably experience leakage due to the existence of the connection interface and are only suitable for the medium and low pressure system. For high pressure system, only

Studies have shown that V acts as a grain refinement in the alloy [11]. V can provide the nucleus for crystallization during the solidification process. If excessive V is present in the melt, a large number of nuclei will be formed. The nucleation elements eventually segregate, which leads to the rapid formation of a large number of dendrites or crystals in the region containing these elements during the initial stage of solidification. A large amount of heat is generated as the latent heat of crystallization, which reduces the degree of subcooling of the liquid metal and promotes grain refinement [12]. Excessive grain formation reduces the content of V in the segregation region, and the diffusion of the V element from other regions to the segregation region is intensified. Finally, it turns exacerbates segregation in this region, the process is shown in Figure 16. Therefore, an appropriate amount of V can refine the grain of the alloy structure, improve the uniformity of distribution of the cast alloy, reduce the segregation of element agglomeration, and strengthen the mechanical properties of the material.

integral casting is chosen. However, the casting temperature of iron is so high that the core sand would be sintered, resulting in deteriorated valve performance. In this study, high performance aluminum alloy is used to form an integrally cast multi-way valve to reduce the difficulty and improve the valve quality, and from which the core sand can be removed easily. The optimal proportions of four alloying elements are determined and the mechanical performance of the alloy is balanced (strength, plasticity, and wear resistance) for hydraulic valve body.

## Acknowledgments

This research was financially supported by the Industrial Research Projects of Guizhou Province, China (GZ NO.[2015]3004). Moreover, this research was also financially supported by the Guizhou Industry Simulation Design & Innovation Center (QKZYD NO.[2016]4006). This research is also support by Doctoral Research Foundation of Guizhou Normal University (2017). This job also support by Experimental Testing and Popularization of Industrial Internet Platforms in the Areas of Guiyang.

## References

- [1] Wang, S.R., Liu, Y.L., Zhu, Y.H., Guo, P.Y. & Wang, M. (2014). Mechanical Properties and Microstructure of Gray Graphite Cast Iron for Cartridge Valve. *Machine Tool & Hydraulics*. 42, 31-34.
- [2] Liu, J.K., Ma, B., Guan, W.J. & Xie, S.Y. (2016). Study on Characteristics of Leakage of Electronic-hydraulic Proportional Multiway Valve. *Machine Tool & Hydraulics*. 44, 120-124.
- [3] Wang, G., Ren, K., Hu, Y.S., Ye, M., Wang, S.Q. & Rong, Y.M. (2018). Microstructural Characteristics-based Mechanical Behavior of Aerospace Al-Cu Alloys. *Journal of Mechanical Engineering*. 54, 77-85.
- [4] Sun, T.F., Wu, Y.Y., Xu, J.J., Guan, B.P., Cao, G.R., Zhou, Q.H. & Gao, Z.Q. (2017). Metal mold gravity casting of high strength Al-Cu alloy. *Ordinance Material Science end Engineering*. 40, 35-38.
- [5] Zhang, X.G., Ma, Y.T., Gui, Z.Y. & Jin, J. (2008). Effect of Zr on Microstructure and Mechanical Properties of 7050 Aluminum Alloy. *Materials for Mechanical Engineering*. 32, 69-71+75.
- [6] Li, Y.Y., Guo, G.W., Zhang, W.W. & Luo, Z.Q. (2002). Effects of Zr and V on Mechanical Properties of Al-Cu Alloy. *Special Cast and Nonferrous Alloys*. 3, 4-6+3.
- [7] Gong, L.Q. (1987). *Metallographic map of cast aluminum alloy*. Changsha: Central South University of Technology Press, 1987.09:41
- [8] Sun, Y.Z., Cao, G. Zhang, G.Q. & Li, C.S. (2000). Cd Strengthening of High Strength Al Alloy. *China Foundry Machinery & Technology*. 6, 20-23.
- [9] Mondolfo, L.F. (1976). *Aluminum alloys: Structure and Properties*.
- [10] Yang, L.Q., Xu, J., Liu, G.J. & Fan, Z. (2012). Microstructural Features of Semi-Solid A357 Alloy Slurry under High-Shear Melt Processing. *Foundry*. 61, 143-146.
- [11] Lu, S.S, et al. (1986). *Nonferrous casting alloys and smelting*. Beijing: National Defense Press.
- [12] Yuan, F.Q., Zhang, J. & Fang, C. (2012). Effects of Rare Earth Addition on Grain Refinement of Magnesium Alloy. *Hot Working Technology*. 41, 30-33+37.